On the Self-Assembly of Monoolein in Mixtures of Water and a Polar Aprotic Solvent

Anna Imberg,*,† Hans Evertsson,† Peter Stilbs,‡ Manfred Kriechbaum,§ and Sven Engström†

Pharmaceutical Physical Chemistry, Department of Pharmacy, Uppsala University, P.O. Box 580, SE-751 23 Uppsala, Sweden, Physical Chemistry, The Royal Institute of Technology, 100 44 Stockholm, Sweden, and Institute of Biophysics and X-ray Structure Research, Austrian Academy of Sciences, A-8042 Graz, Austria

Received: August 7, 2002; In Final Form: November 13, 2002

Four different one-phase regions: two liquid phases (L and L_3) and two liquid crystalline phases (L_α and V_2) of the MO/NMP/water system, were studied by SAXS, PGSE-NMR, and rheology at 20 °C. The location of the dramatic increase in solubility of MO, in binary NMP/water mixtures, can be explained in terms of the presence or absence of free water, as a consequence of strong NMP(water)$_2$ complex formation in the binary NMP/water system. A direct effect of this complexation is aggregate formation at a certain region within the L phase. The microstructure of the L_3 phase can be modeled as bicontinuous according to the theory of interconnected rods when formation of NMP(water)$_2$ complexes are taken into consideration. The swelling of the sponge phase correlates well to predicted swelling laws and characteristic lengths, as found in other sponge phases. The cubic phase region of the ternary system consists of at least two different cubic phases, with $Pn\bar{3}m$ and $Ia\bar{3}d$ symmetry of the space group, respectively. At higher NMP contents it seems as if the $Pn\bar{3}m$ symmetry of the space group transforms into $Im\bar{3}m$.

Introduction

Monoolein (MO), a metabolite during fat digestion in the upper intestine, has due to its peculiar phase behavior in water received much interest in the biotechnical field. In excess water, MO forms a bicontinuous cubic liquid crystal, which consists of one congruent lipid bilayer extending in three dimensions surrounded by (two) water channel systems.[1] The stiff cubic phase has been used as a drug delivery vehicle,[2] and as a matrix for water-soluble proteins in a biosensor application.[3]

In 1996, Landau and Rosenbuch showed that the cubic phase also can act as a "solvent" for the membrane protein bacteriorhodopsin (bR) from which bR crystals could be obtained.[4] Although a promising system, the cubic phase has not turned out to be a universal tool for membrane protein crystallization, and to date, structures of less than 10 different membrane proteins from crystals have been published with the so-called in cubo method.[5] One reason for this, as pointed out by Rummel et al.,[6] may be the relatively narrow water channels in the cubic phase (about 50 Å in the fully swelled state) that may prevent membrane proteins with large extrabilayer parts to be incorporated in the system.

There are a number of ways to widen the water pores of the cubic phase. One is to add a slight amount of a charged phospholipid[7] or a bile salt;[8] another is to add a block copolymer such as poloxamer 407 (polethylene oxide−polypropylene oxide−poly(ethylene oxide)).[9] Recently, it was shown that simple inorganic salts such as NaSCN and NaI are able to increase the size of the water channels considerably at concentrations below 1 M.[10] The mechanisms behind the water swelling of the cubic phase should be very different for the three cases mentioned above, because, e.g., the lipid exerts its effect in the bilayer whereas the polarizable anions of the salts probably partly adsorb at the interfacial layer in the phase.

An additional way to swell the cubic phase is by adding certain types of water-miscible solvents to the MO/water system. Examples of such solvents are dimethyl sulfoxide (DMSO),[11] propylene glycol (PG),[11,12] ethanol (EtOH),[11,13] poly(ethylene glycol) (molecular weight 400, PEG 400),[11,12] 2-methyl-2,4-pentanediol (MPD),[13] and *N*-methylpyrrolidinone (NMP).[13,14] These solvents all have in common that they are totally miscible with water and freely miscible with monoolein. The most thoroughly investigated solvent is NMP, and the three-component phase diagram MO/NMP/water is given in Figure 1.[14] One important property of NMP in water is that it forms a strong NMP(water)$_2$ complex.[15,16] It turns out that this complex formation has a profound effect on the self-assembly of monoolein in NMP/water mixtures. In this work we present structural and dynamical data obtained from NMR, viscosity, and X-ray measurements. The results are discussed in view of the NMP(water)$_2$ complex. It should be noted that the interpretation given for NMP may well be relevant for several of the other solvents mentioned above as well, e.g., DMSO.

Materials and Methods

Materials. Rylo MG 19 Pharma (lots 2119/54 and 1876/88) was kindly provided by Danisco Cultor (Brabrand, Denmark). The monoglyceride content was 98.1% and 94.9%, respectively. The rest was mainly free glycerin. The monoolein part of the monoglycerides was 90.3% and 88.4%, respectively. The following chemicals were purchased from Sigma Aldrich:

* Corresponding author. E-mail: anna.imberg@farmaci.uu.se. Fax: +46184714377.
† Uppsala University.
‡ The Royal Institute of Technology.
§ Austrian Academy of Sciences.

10.1021/jp021829y CCC: $25.00
Published on Web 02/12/2003

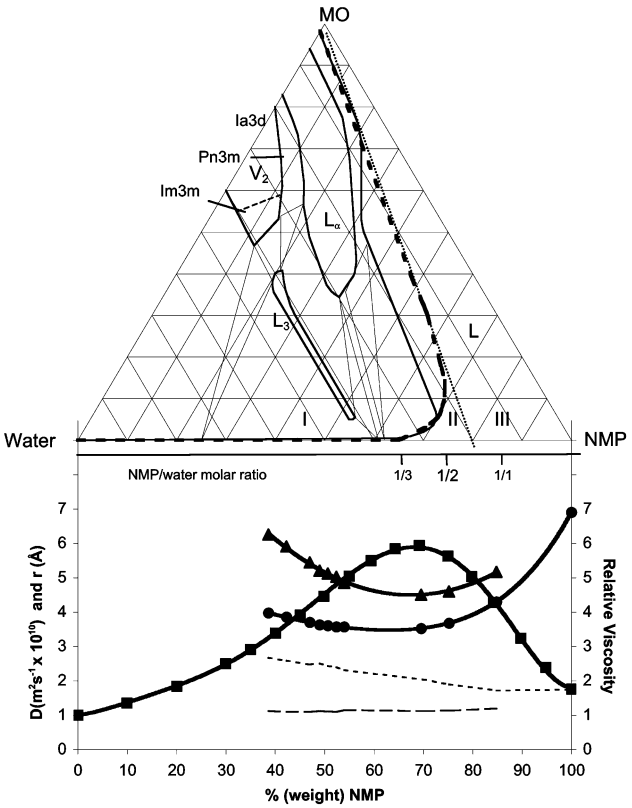

Figure 1. Phase diagram (solid lines) of MO (batch no./lot no. 1876/88)/NMP/water system at 20 °C (top). The calculated phase boundary, according to Flory−Huggins theory (dashed line) and the solubility limit of MO (dotted line), are also shown (top). The self-diffusion coefficients of water (filled triangles), NMP (filled circles), and the relative viscosity (filled squares) of the binary NMP/water system at 20 °C (bottom). The latter is related to the viscosity of water at 20 °C. The calculated hydrodynamic radii of NMP (short dashed line) and water (long dashed line) are also shown (bottom).

ethyl acetate (EtAc) (analytical reagent, Riedel-de Haën) and 1-methyl-2-pyrrolidinone (NMP) (anhydrous grade, Aldrich). Millipore filtered water was used in all samples for X-ray and rheology measurements. Deuterated water (99.9%) was purchased from Isotech Inc. (Miamisburg, OH). Vials for the robotic liquid handler were bought from NTK Kemi (Uppsala, Sweden) and from Scantec Lab AB (Partille, Sweden). Silicon plugs with aluminum casings were used for sealing of the vials. All reagents were used as supplied.

Sample Preparations. Samples for most of the X-ray measurements were prepared by means of a robot (Gilson, Liquid Handler) in such a way that every sample weighed 0.3 g. A mixture of 40% MO and 60% EtAc was dispensed, at 22.0 °C, by the robot into previously weighed vials. The vials were left open, at 40 °C, thus allowing ethyl acetate to evaporate. Water was added to the vials when the ethyl acetate content had become less than 0.5%. NMP was added by using a syringe with a needle to inject through the silicone plugs of previously sealed vials. The samples were weighed before and after each addition to check that ethyl acetate had evaporated and that the robot had dispensed the correct amounts. The samples were vortexed and then centrifuged in a Beckman Avanti 30 compact centrifuge (Palo Alto, CA). All samples reached equilibrium conditions within days to a few weeks. The anisotropy of the samples were studied between crossed polarizers. A manuscript describing development and validation of this method is submitted.

The samples for the FT PGSE NMR, rheology, and viscosimetry measurements were prepared by weighing appropriate amounts of MO, NMP, and water in glass vials, which were directly sealed. The samples were centrifuged, at approximately 9400 g (20.0 °C, 10−20 min) in a Beckman Avanti 30 compact centrifuge (Palo Alto, California), to enhance mixing and equilibration. The samples were then equilibrated (days to weeks) before any measurements were performed.

Fourier Transform Pulsed Field Gradient Spin−Echo NMR (FT-PGSE NMR). Fourier transform pulsed-field-gradient spin−echo NMR[17] was used to simultaneously measure the lateral self-diffusion coefficient of MO, NMP, and water. In the stimulated echo pulse sequence (STE) used here,[18] three 90° pulses are separated in time by delays τ_1 and τ_2, and two magnetic gradient pulses are separated by time Δ. The rf pulses were cycled in a 8-step fashion, to suppress other echoes and to even out internal spectrometer channel mismatches. The echo amplitude, A, at time $\tau_1 + \tau_2$ is dependent on the diffusion coefficient D according to

$$A(\tau_1 + \tau_2) = 0.5A(0)\exp\left(-(\tau_2 - \tau_1)/T_1 - 2\tau_1/T_2 - (\gamma g\delta)^2 D\left(\Delta - \frac{\delta}{3}\right)\right) \quad (1)$$

where $A(0)$ is the amplitude at time 0, T_1 and T_2 are the longitudinal and transverse relaxation times, respectively, and γ is the magnetogyric ratio. g is the intensity and δ the duration of the gradient pulses. By varying g between 0.1 and 2.9 T m^{-1} and keeping δ and Δ constant at 2 ms and 220 ms, respectively, D was separated from the transverse relaxation effect. A total of 16 or 32 such echoes were time-averaged and then Fourier-transformed for each g value. PGSE-NMR measurements were performed on a Bruker AMX 300 spectrometer equipped with a wide-bore magnet and a dedicated diffusion probe head from Cryomagnet systems, Indianapolis, IN, and a gradient driver made by W. S. Woodward, University of North Carolina, Chapel Hill, NC. NMR data were evaluated by the CORE-NMR (COmponent REsolved NMR) approach by Stilbs et al.[19] CORE is a global minimization procedure using all spectral information rather than single peak heights, which, in addition to the possibility of resolving partly overlapping spectral peaks, gives an enhanced signal-to-noise ratio of about 10. The temperature was set to 293 ± 0.2 K by the temperature control program. Diffusion coefficients were measured and successfully fitted to a simple Gaussian process, even at 100% attenuation of the echo signal, with an experimental error of better than ±5%.

Rheology. The rheological experiments were carried out using a Bohlin VOR Rheometer (Bohlin Reologi, Lund, Sweden), a controlled rate instrument of the couette type. A concentric cylinder measuring system, C14, was used. To prevent evaporation, a lid was used during the measurements. Samples (2.6 mL) were used for every experiment. Data were collected and evaluated with the software VOR Millenium (Bohlin Reologi, Lund). The temperature was controlled by a temperature control unit (Bohlin Reologi, Lund). The viscosities were determined at 20.0 °C. All samples were equilibrated for 15 min before the experiments started.

The viscosities of binary mixtures of NMP and water were determined relative to the viscosity of water with an Ubbelodhe viscometer (Cannon Instrument company, 100/L101). Before the tests were carried out, the viscometer, with 2 mL samples, was tempered to 20.0 °C for 15 min. Viscosities were determined by 5 consecutive tests, all within 0.20 s margin.

Small-Angle X-ray Scattering (SAXS)/Small-Angle X-ray Diffraction (SAXD). A modified Kratky compact camera (HECUS MBraun, Graz, Austria) was used for SAXS and SAXD analysis. X-rays were generated by a Philips PW1830/40 generator operating at 50 kV and 40 mA, equipped with a Cu-target sealed X-ray tube producing Cu Kα radiation with a wavelength of 1.542 Å. A 1D, position-sensitive wire-detector (OED 50M, MBraun, Garching, Germany) was used for detection of scattered and diffracted X-rays in the small-angle region. A peltier element, PC-controlled by the software MTC version 4.2 (HECUS MBraun, Graz, Austria), was used for temperature stabilization and control of the sample. Cubic and lamellar phases were X-rayed in a sample holder in which the samples were placed between two thin mica sheets. L and L_3 phases were X-rayed in quartz capillaries with a diameter of 1 mm. All samples were equilibrated at 20.0 °C for 300−900 s before the X-ray measurements started. Exposure times of the samples were chosen between 1800 and 200 000 s. The evaluation of data was aided by the software 3D-View (version 4.1).

Results and Discussion

The phase diagram of the MO/NMP/water system is given in Figure 1. To emphasize the importance of the microstructure of the NMP/water system, the phase triangle rests on the water/NMP side. At room temperature the system exhibits four different one-phase regions: two liquid phases (L and L_3) and two liquid crystalline phases (L_α and V_2). The cubic region (V_2) consists of at least two different cubic phases with different space groups; see below.

Binary NMP/Water System. Figure 1 shows the relative viscosity of the NMP/water system together with self-diffusion coefficients, *D*, for water and NMP, respectively. It is evident from the figure that all three data sets show extreme values around 70% NMP, close to the NMP/water molar ratio 1/2 (i.e., 73% w/w NMP). The relative viscosity is in good agreement with earlier reported results obtained at 25[15] and 30 °C.[16] The maximum in the viscosity curve was taken as one of several indications of the existence of a strong NMP(water)$_2$ complex.[15]

In view of the complex formation we may also understand the minima obtained in the self-diffusion of water and NMP, respectively. The diffusion data are analyzed within the Stokes−Einstein approximation, given by

$$D = \frac{kT}{6\pi\eta r} \tag{2}$$

where η is the viscosity and *r* is the radius of a diffusing sphere. *T* and *k* carry their usual meaning. We see from Figure 1 that reasonable values and concentration dependencies of *r* are obtained if one assumes diffusing spheres of water, NMP, and the NMP(water)$_2$ complexes.

A striking effect of the NMP(water)$_2$ complex formation is the behavior of the solubility of MO in NMP/water mixtures. It increases dramatically around 73% NMP, as is shown by the phase boundary of the L phase, if interpreted as a MO solubility curve, in Figure 1. Below 65% NMP content the MO solubility is less than 1%, and in the region with 65−73% NMP content the solubility reaches about 5%, followed by total miscibility of MO at NMP contents higher than 80%. A reasonable interpretation of this behavior is that the fraction of free water molecules starts to become negligible at 73% NMP content due to the strong complex formation of water with NMP. The increasing fraction of free NMP molecules above 73% readily dissolves MO because NMP and MO are (almost) totally miscible. This interpretation is similar to the interpretation reported by Hong and Huang,[16] who studied the conformation of poly(vinyl alcohol) (PVA) in mixtures of NMP and water. The three different water/NMP regions discussed above are given in Figure 1 by roman numerals. The characteristics of each region is as follows: NMP/(water)$_2$ complexes coexist with free water molecules (region I), in the transition region (region II) the amount of NMP(water)$_2$ complexes dominates compared to the amount of free NMP and water molecules present, and at higher NMP contents, only free NMP molecules are coexisting with NMP(water)$_2$ complexes (region III). Thus the solubility of MO can be understood from the complexes formed in the binary NMP/water system; i.e. when there are no free water molecules present, MO is totally soluble (see Figure 1).

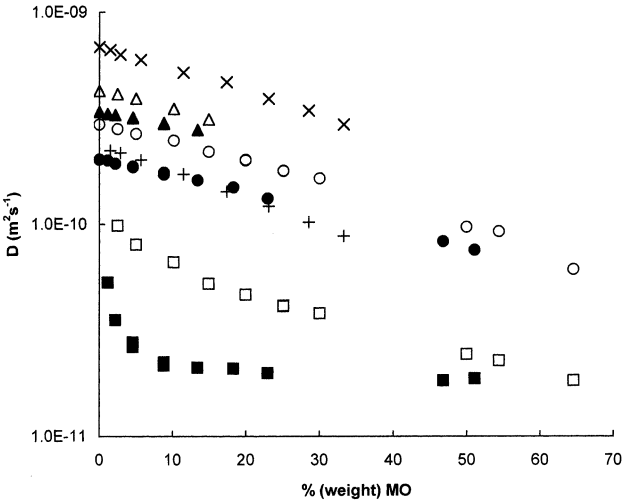

Figure 2. Self-diffusion coefficients of water (triangles), NMP (circles and crosses), and MO (squares and pluses) of three series of samples, at varying water/NMP ratios: 0.18 (open symbols), 0.33 (filled symbols), and 0 (crosses and pluses), in the ternary L region of the MO (batch no./lot no. 1876/88)/NMP/water system.

Liquid Phase of the Ternary MO/NMP/Water System. The large liquid region, denoted L in Figure 1, extends from the water corner to the MO corner of the phase diagram. The dashed line, shown in the L region, is obtained from a one-parameter fit to an earlier Flory−Huggins calculation of the phase behavior of a quaternary system including the MO/NMP/water subsystem.[14] The Flory−Huggins model is able to give a good description of the MO-poor and MO-rich parts of the L region but is unable to describe the MO-rich L phase-boundary between 5% and 75% MO. This is not unexpected, since the Flory−Huggins model assumes random mixing of the components, whereas the present system gives rise to several phases with ordered structures. The question is, if the spatial discrepancy between the calculated Flory−Huggins phase boundary and the experimentally determined phase boundary at region II, implies a more ordered structure in the water rich L region. To investigate this hypothesis, a series of experiments were undertaken with samples from various parts of the L region.

The self-diffusion for MO, NMP, and water in the L region at different NMP/water ratios are given in Figure 2 as functions of MO content. It can be seen from Figure 2 that the diffusion coefficients of NMP and water decrease almost linearly with MO content, which is a direct consequence of the corresponding increase in viscosity. In the binary MO/NMP system, the diffusion of MO is also affected by the increase in viscosity. In the presence of water, however, the decrease in the diffusion coefficient of MO is strongly nonlinear with respect to the MO content. For comparison, the MO diffusion at the highest water

content (water/NMP = 0.33) approaches the diffusion coefficient obtained in the sponge phase. From Figure 2 it is clear that the diffusion coefficient of MO, at water/NMP = 0.33 and at low MO contents, is rapidly reduced as the MO content increases. This drastic decrease in the lipid diffusion coefficient resembles the decrease in diffusion of a surfactant as CMC is reached in a dilute surfactant system; see for example ref 20. The normally accepted two-state mass balance equation describing how the observed diffusion coefficient varies as a function of the diffusion coefficients of free monomers and micelles in a dilute surfactant system,[20] can be written as

$$D_{obs}C_{tot} = D_{agg}C_{tot} + (D_{free} - D_{agg})C_{free} \qquad (3)$$

D_{obs}, D_{free}, and D_{agg} are the observed average, free surfactant, and aggregated surfactant self-diffusion coefficients, respectively. C_{free} and C_{agg} are the concentrations of free surfactants and aggregated micelles, respectively. C_{tot} is the total concentration of surfactant, i.e., $C_{tot} = C_{free} + C_{agg}$. In this simple model, a linear fit of $D_{obs}C_{tot}$ versus C_{tot} reveals if C_{free} is constant. If MO aggregates, it is possible that the concentration dependence of the diffusion coefficient, given in eq 3, may be more complex. However, when this model was applied on the data presented here, with the highest water content (water/NMP = 0.33), D_{agg} was determined from the slope to be 1.77×10^{-11} m^2/s. Estimating the limiting MO diffusion coefficient at zero MO concentration gives the free MO diffusion coefficient D_{free}, corrected for the viscosity of the medium water/NMP = 0.33. This was done by fitting the limiting values of D_{free} at water/NMP = 0 and 0.18 as a function of the relative viscosity and extrapolating to water/NMP = 0.33 (because the MO diffusion coefficient curve at water/NMP = 0.33 in Figure 2 is strongly nonlinear and not easy to fit directly). D_{free} may this way be estimated to 7.6×10^{-11} m^2/s. This finally gives a viscosity-corrected critical aggregation concentration of MO of 19 mM, at water/NMP = 0.33.

In conclusion, the NMR self-diffusion measurements of the L phase monitors random mixing at zero and low water content, an intermediate zone at water/NMP = 0.18 where NMP(water)$_2$ complexes and free water starts to affect the data, and a zone possible to model as a simple micelle solution at water/NMP = 0.33. The "solvent" NMP/water hence becomes "less good" for MO as the NMP content and thus the number of free NMP molecules decreases. The compositions of the samples at water/NMP = 0.33 are located inside the two-phase region of the calculated Flory−Huggins phase boundary, but outside the corresponding experimental phase-boundary; i.e., the NMP/water ratio matches the above-mentioned region II. The spatial discrepancy between the experimental and calculated phase boundary originates in aggregate formation within the L phase. The diffusion coefficient of MO aggregates is 1.8×10^{-11} m^2/s at water/NMP = 0.33 as calculated above. The viscosity of water/NMP = 0.33 is some 5 times larger than that of pure water, as can be seen from Figure 1. The diffusion coefficient of the MO aggregate in a liquid of the same viscosity as water should thus be approximately 1×10^{-10} m^2/s, which is comparable to the diffusion coefficient of ordinary SDS micelles in water. The diffusion data presented here do not contain any information of the shape of the aggregates formed.

In a series of samples with constant MO/NMP ratio (20/17 w/w) the effects caused by addition of water on X-ray scattering data as well as viscosity were determined. The X-ray diffraction peaks, shown in Figure 3, are broad but narrow as water is added. The positions of the peaks correspond to characteristic lengths of an order of magnitude typical for bilayer-like

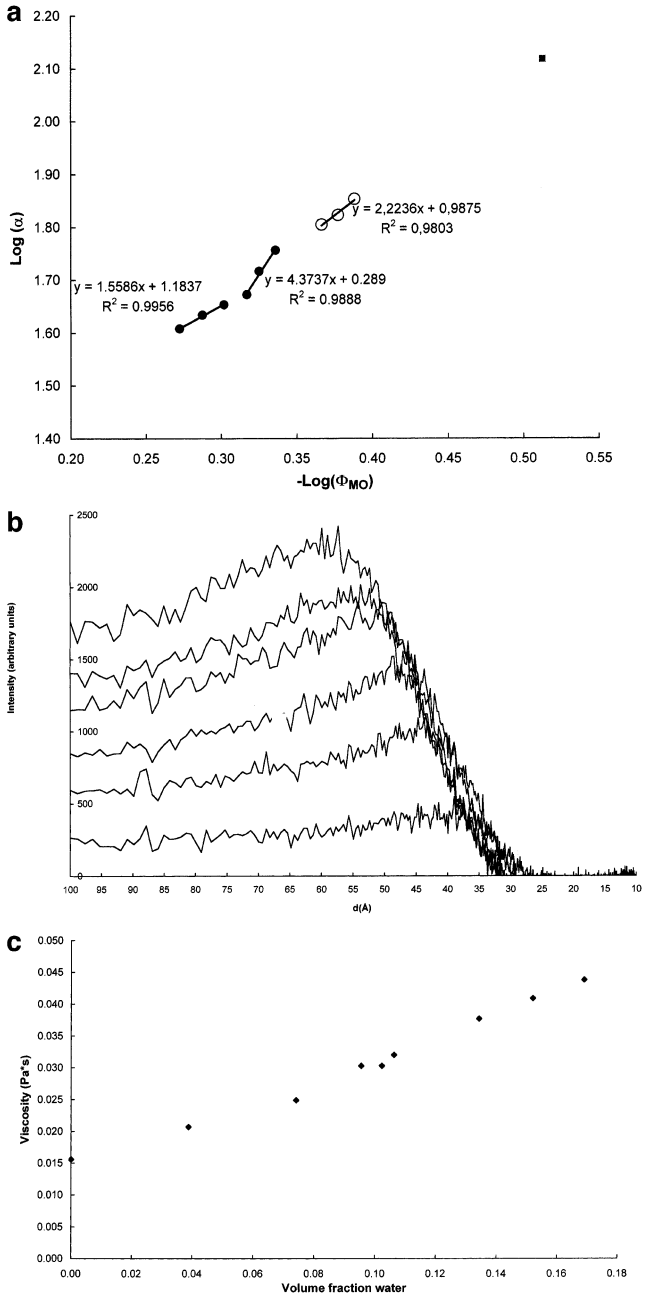

Figure 3. SAXS/SAXD data of a series of samples L (filled circles), L_α (open circles), and L_3 (filled square) with constant MO (batch no./lot no. 2119/54)/NMP ratio (20/17 w/w) (a). The SAXS spectra, of the samples of the L phase, is illustrated in (b) where the intensity of a binary MO/NMP (20/17 w/w) sample has been subtracted from the measured intensities, and the corresponding results from the rheology measurements of the L phase are shown (c), of the MO (batch no./lot no. 2119/54)/NMP/water system.

structures. As shown in Figure 3, both the intensities and the characteristic lengths vary with varying water content. The peak positions shift to higher angles with increasing water content, indicating increased bilayer thickness. The observed change in intensity might be due to an increased number of bilayer-like aggregates. However, the intensity can also change due to changes in electron density.

If the lattice parameters (α) are plotted vs volume fraction MO (ϕ_{MO}) in a log−log-plot, the slopes of the curve follow the sequence 1.6−4.4−2.2 as water is added (if a perfect one-dimensional swelling would prevail, the slope should be 1). It turns out that, the three swelling regions matches the three NMP/

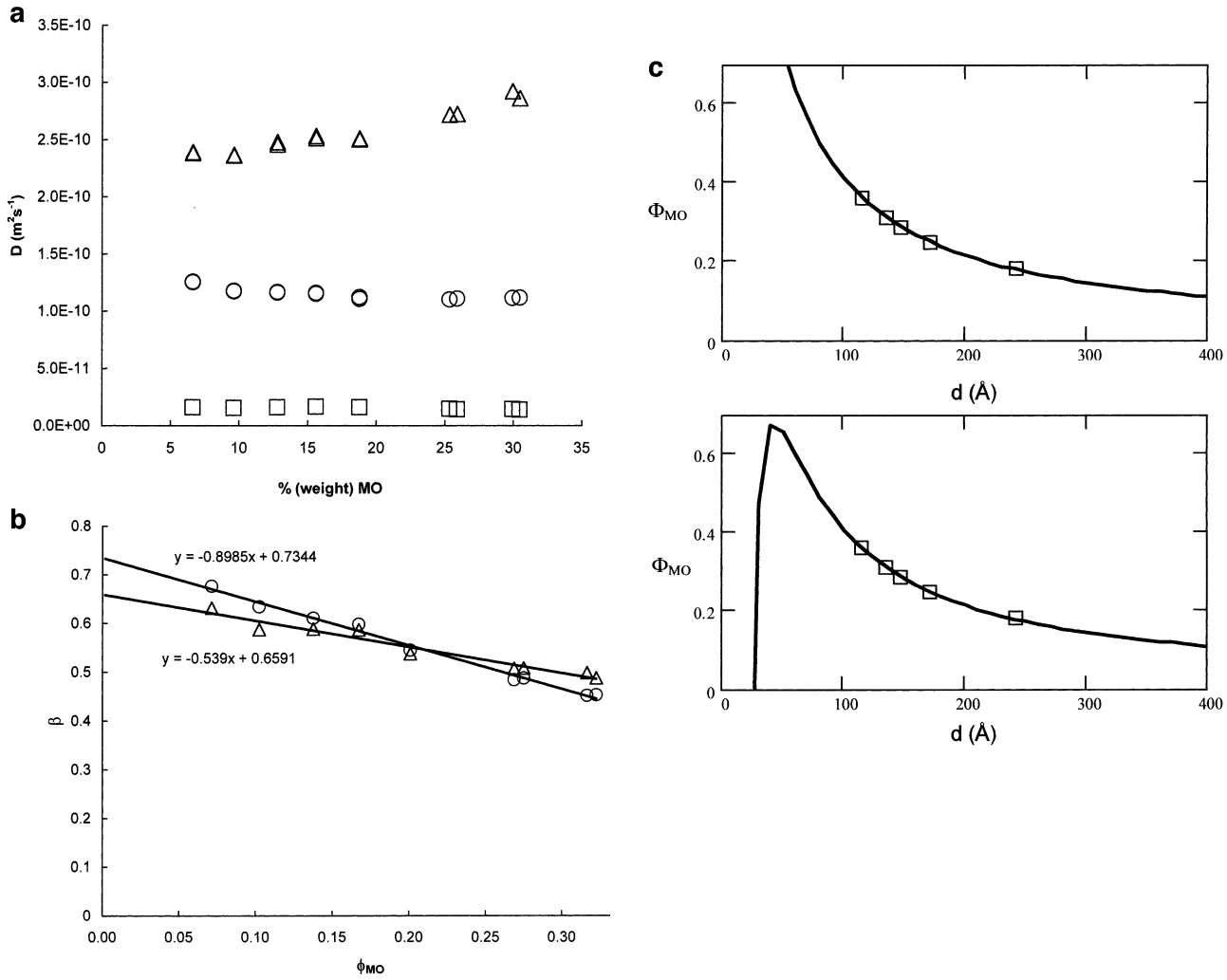

Figure 4. Self-diffusion coefficients of MO (squares) (batch no./lot no. 1876/88), NMP (circles) and water (triangles) within the L_3 phase (a) and obstruction of NMP (circles) and water (triangles) versus Φ_{MO} (b). The swelling of the L_3 phase of the MO (batch no./lot no. 2119/54)/NMP/water system is shown in (c). Experimental data (squares) and the best fittings (lines) according to eq 5 (top) and 6 (bottom) are given.

water regions described above. A possible interpretation of the X-ray data of Figure 3 is as follows:

(i) As water is added to the NMP/MO mixture corresponding to region III according to Figure 1, NMP(water)$_2$ complexes start to form and probably accumulate close to the polar region of MO. Broad diffraction peaks appear and the slope is higher than 1 because of the rearrangement of NMP in the system.

(ii) As more water is added to the NMP/MO mixture corresponding to region II in Figure 1, free NMP disappears and free water appears. A rearrangement of MO−NMP interactions to MO−MO interactions becomes necessary to minimize the free energy of the system. The result is a three-dimensional swelling probably by formation of bilayer-like aggregates. The region can so be modeled as a simple micellar solution, as shown above. The slope in Figure 3a is then again lower in the lamellar region, and this phase swells in a one-dimensional manner when a certain NMP/water mixture is added (see below).

Sponge Phase. The bicontinuous sponge (L_3) phase in this system is a narrow phase region stretched out at a constant water content of about 42 wt %, thus allowing a variation in lipid and NMP contents; see Figure 1. The closely related L_3 phase of the system MO/PEG 400/water has been shown to be bicontinuous, as monitored by conductance[13] as well as NMR self-diffusion.[21] It was shown that the MO/PEG 400/water L_3 phase can be modeled as bicontinuous under the assumption that the lipid forms one subdomain and the water forms the other with PEG dissolving almost quantitatively in the water domain. It is therefore reasonable, as a first approximation, to assume that NMP quantitatively dissolves in the water subdomain of the L_3 phase.

NMR self-diffusion data of the MO/NMP/water L_3 phase are given in Figure 4. It can be seen from the figure that as the MO content increases, the diffusion coefficient of water in L_3 also increases. This is an effect of the corresponding increasing curvature of the lipid membrane, allowing straighter diffusion paths within both domains, because more "connective points" become accessible. However, the data are affected also by the specific NMP(water)$_2$ complexation. As the MO content in L_3 increases, the NMP content decreases, resulting in more water not bound to NMP (see the binary NMP/water system above). This also increases the water diffusion coefficient. Consequently, as the NMP content decreases, the fraction of NMP bound to water increases, lowering the NMP diffusion coefficient somewhat with increasing MO content.

Bicontinuous structures can be modeled according to the theory for interconnected rods, the ICR model.[22] The ICR model for an L_3 phase is approximated by[23]

$$\beta = 0.636 - 0.264\phi_{\text{bilayer}} \qquad (4)$$

β is the obstruction factor and ϕ_{bilayer} is the volume fraction of the bilayer. (If the obstruction factor equals 1, the obstruction of diffusion is 0.) The approximation was recently used on the L_3 phase of the MO/PEG 400/water system,[21] and earlier on the L_3 phase in the AOT/NaCl/water system.[24] Here, we have modeled the sponge phase in the MO/NMP/water system, within the ICR model, assuming that the volume fraction of the bilayer equals the volume fraction of MO ($\phi_{\text{bilayer}} = \phi_{\text{MO}}$) The obstruction factors, at zero volume bilayer of NMP and water were determined from a linear fit (β vs ϕ_{MO}), to 0.73 and 0.66, respectively, as can be seen in Figure 4, which is close to the ideal value of 0.636. The structure of L_3 may thus be described as bicontinuous. The obstruction factors of NMP and water are both slightly higher as compared to the obstruction factors of PEG 400 and water in the corresponding MO/PEG/water system. This suggests a less restricted diffusion in the present MO/NMP/water system, a result not too surprising taking into consideration the molecular weight of PEG 400 as compared to that of NMP. The higher limiting obstruction (less restricted diffusion) of NMP as compared to water in the MO/NMP/water system suggests NMP to have some small partition to the lipid bilayer, utilizing both subdomains as diffusive media, although with a strong preference for the water subdomain.

The swelling of L_3 as monitored by X-ray scattering, when assuming that $\phi_{\text{MO}} = \phi_{\text{bilayer}}$, is shown in Figure 4. The characteristic lengths are of the same order of magnitude as in other sponge phases.[13,24−26] The oil and water domains are well-separated in other sponges such as water/Nacl/pentanol/sodium dodecyl sulfate,[25] water/dodecane/pentanol/SDS, and water/NaCl/sodium bis(2-ethylhexyl) sulfosuccinate.[24,26] These systems may therefore be regarded as more ideal sponge phases as compared to the present one, where the solvent NMP is miscible with both oil and water. As shown above by means of NMR, NMP distributes almost quantitatively in the water domain.

The swelling of the sponge phases has been described theoretically in two different ways.[27] For dilute systems, one can interpret the swelling geometrically, under the assumption that the laws of swelling apply approximately. The swelling, at constant average molecular shape, is given by

$$(1 - \phi)^{S_{\text{in}}} = K\left(1 - \frac{C_1}{d}\right) \tag{5}$$

where ϕ denotes the volume fraction of bilayer, S_{in} is the inner shape parameter, and d is the characteristic length of the sponge. $C_1 = (-2\pi\chi/H)^{1/3}l$, where H denotes the homogeneity index, i.e., a dimensionless measure of surface-to-volume ratio, and χ is the Euler−Poincaré index, which is a property of the topology.[27] K is a constant. The chain length, l, is approximately 17−20 Å for MO.[13,27,28]

Swelling while a neutral surface is maintained at a fixed distance from the midsurface of the bilayer is described[27] by

$$\phi_{\text{MO}} = C_2 d^{-1} + C_3 d^{-3} \tag{6}$$

H and χ_{d} can be determined from the two constants C_2 and C_3.[27]

From Figure 1, it is evident that the sponge phase can coexist with the cubic phase. Both phases are bicontinuous and the sponge phase can, in fact, be regarded as a swollen, melted cubic phase. To relate the topology of the sponge phase in the MO/NMP/water system to the cubic minimal surfaces, we have fitted our data according to eqs 5 and 6, respectively; see Figure 4. The results from the fitting procedure of smeared data are $\chi_{\text{d}} = -0.52$, $H = 0.70$, and $S_{\text{in}} = 0.64$. It should be noted that the characteristic lengths are somewhat overestimated due to smearing. However, these results indicate that the sponge phase is closely related to the cubic phase and it seems as if the structure found in the solvent-poor part of the sponge phase is similar to the structure of the P surface. The Euler−Poincaré index of a restricted volume ($hkl = 200$) of the P surface is −0.50.

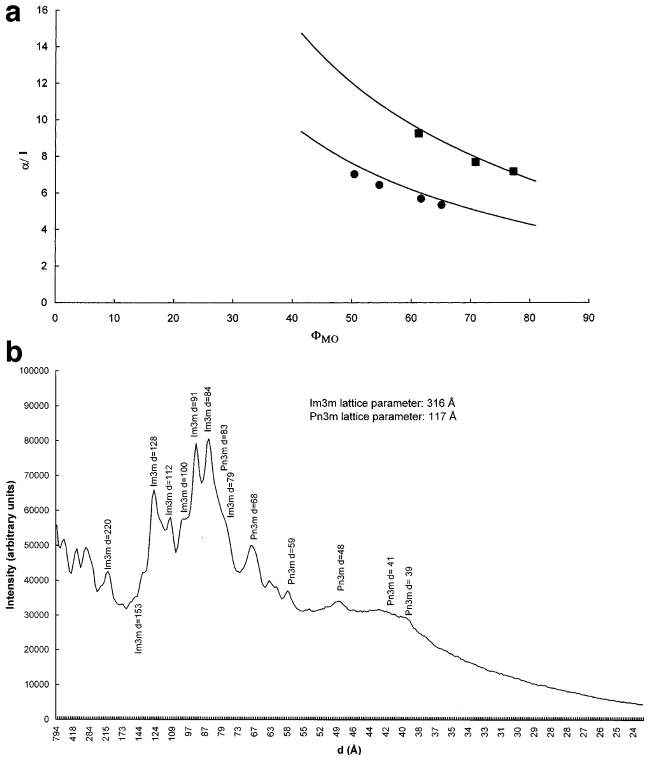

Figure 5. Swelling of the G surface (squares) and of the D surface (circles). The solid lines illustrate the predicted swellings when $l =$ 17.9 Å (a) and one representative SAXD spectra of the $Im\bar{3}m/Pn\bar{3}m$ sample of the MO (batch no./lot no. 2119/54)/NMP/water system (b).

Cubic Phase(s). It is well-known that the Schwarz' double diamond surface, the D surface ($Pn\bar{3}m$), exists in equilibrium with excess water in the binary MO/water system. At lower water contents, the D surface transforms into Schoen's gyroid surface, the G surface ($Ia\bar{3}d$). The P surface does not exist in the binary MO/water system. The volume per unit surface, $V^{2/3}/A$, for the P, D, and G surfaces are 1.07, 1.02, and 1.00, respectively.[29] The P structure cannot be present in the binary MO/water system because the cubic structure in the binary MO/water system is not swollen enough (i.e., the bilayer content per unit cell is lower in the P structure as compared to the D structure) to form the P surface.[29] However, when proteins are present in the water channels (i.e., when the bilayer takes up a smaller part of the unit volume), the water swelling of the cubic phase increases, and the P structure can be formed in the MO/water system.[30,31]

The solvents used in the MO/solvent/water systems are mainly located within the water domains, and hence the swelling of the cubic phase increases. Therefore, it seems reasonable that the P surface may be induced by addition of solvents such as NMP, PEG 400, or DMSO. Figure 5 illustrates the swelling of the cubic phases where samples from both the binary MO/water and the ternary MO/NMP/water system have been used. As expected, the D surface ($Pn\bar{3}m$) exists in equilibrium with excess water in the binary system. At lower water contents, the D surface transforms into the G surface ($Ia\bar{3}d$). Figure 5

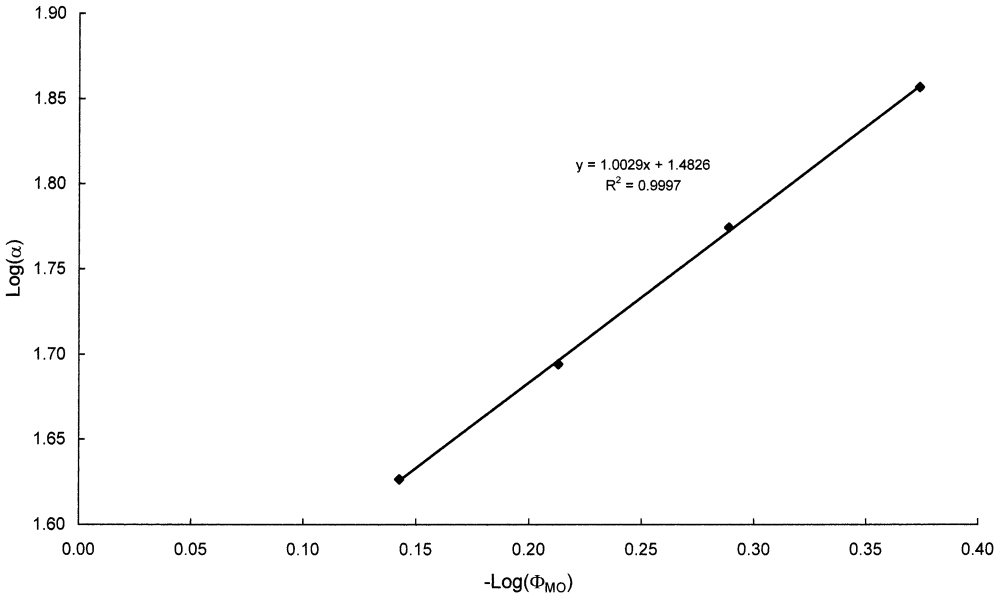

Figure 6. 1D swelling of the lamellar phase of the MO (batch no./lot no. 2119/54)/NMP/water system. The samples have a constant NMP/water (50/50 w/w) ratio.

illustrates that the swelling of both these surfaces corresponds well to the predicted theoretical swelling,[28] given by

$$\frac{\alpha}{l} = \left(\frac{2\pi\chi}{H}\right)^{1/3}\sqrt{3}\sin\left(\frac{\Delta}{3}\right) - \cos\left(\frac{\Delta}{3}\right)^{-1} \tag{7}$$

where

$$\Delta = \pi + \frac{a\tan\sqrt{(1-\phi_{MO})^2}}{-\phi_{MO}} \tag{8}$$

and χ is the Euler characteristic, defined as $2-2\times$ genus. The genus is 5 for the G surface and 2 for the D surface. H is the homogeneity index, α is the lattice parameter, and l denotes the chain length.

Equation 7 applies to a binary system, where the water domain is separated from the oil. The ternary MO/NMP/water system is here regarded as a pseudobinary system. Because the NMP content of the cubic region of the phase diagram of Figure 1 is small, less than 15 wt %, the partition of NMP to the lipid is here neglected. The swelling of the D and G surfaces of the ternary system, which is in good agreement with theory, is illustrated in Figure 5. The G surface does not exist at higher NMP contents. When the NMP content of the cubic phase is increased, the D surface is probably transformed into a surface with $Im\bar{3}m$ symmetry of the space group; see the schematic phase boundary in Figure 1. Both the P, the I-WP, and the Neovius (C(P)) periodic minimal surfaces have this space group. One representative SAXD spectra from the two-phase region ($Im\bar{3}m$ $\alpha = 316$ Å, $Pn\bar{3}m$ $\alpha = 117$ Å) is shown in Figure 5. In this sample, also some peaks are seen at very low angles, which could be from another $Im\bar{3}m$ cubic phase, with a large lattice parameter (>500 Å). The order of magnitude of the former lattice parameter of the $Im\bar{3}m$ structure corresponds well to the Neovius C(P) samples measured in the monoglycerides/poloxamer 407/water system.[9] However, it should be noted that it is tricky to determine which cubic phase(s) are present in the solvent-rich part of the cubic region. Some extra peaks can be present due to local orientations and some peaks may be canceled out when the structure factor is zero. In fact, it is possible that different cubic phases (see above), with $Im\bar{3}m$ symmetry of the space groups, are present.

The Lamellar Phase. A number of samples within the lamellar L_α phase with constant NMP/water ratio, were examined by means of SAXD. For an ideal lamellar phase, the following relation holds

$$\alpha = \frac{d_{bilayer}}{\phi_{MO}} \tag{9}$$

where α denotes the repetitive distance. The swelling behavior of the lamellar phase is shown in Figure 6. The slope, in Figure 6, is 1.0. The theory behind 1-dimensional swelling[20] assumes that the lamellar phase is built up by two immiscible components, but because NMP is miscible with both MO and water it is not obvious that the slope should be exactly 1. This experiment illustrates that NMP is not present in the MO domain to any extent affecting the one-dimensional swelling of the lamellar phase.

When our samples from the lamellar region were X-rayed at 20 °C, only the first diffraction order was observed, which is not enough to be able to with absolute certainty claim that the phase is lamellar. However, in some samples, the second-order diffraction was observed, although the intensity of that peak was low. Others have also earlier experienced this in similar systems.[32] The phase is here labeled lamellar because it exhibits all the properties of a lamellar phase on the macroscopic level and because it swells in an ideal lamellar way. We have also induced the L_α to L_c (lamellar crystals) transition when cooling some sample to 17−18 °C. In analogy with Borné et al.,[32] the L_c phase showed more diffractions than the L_α phase; i.e., the Bragg spacing ratio was 1:2:3.

Conclusions

The NMP(water)$_2$ complex formation is the origin of nonideality in the binary NMP/water system, and strongly affects the ternary MO/NMP/water system as well. The solvency of MO, in binary NMP/water mixtures, can be understood from the stoichiometric relation between water and NMP. MO readily dissolves in NMP(water)$_2$ with excess NMP. Taking into

consideration the formation of the NMP(water)$_2$ complex, the phases of the MO/NMP/water system can be explained as well. The L_3 phase, for instance, is easily modeled as a bicontinuous structure. The cubic phase region consists of at least two different cubic phases, one with a *Pn*3*m* space group (the D surface) and one with *Ia*3*d* symmetry of the space group (the G surface). At higher NMP contents, it seems as if the *Pn*3*m* space group transforms into a *Im*3*m* symmetry, a P surface, which is logical as this symmetry, is possible at a higher degree of swelling.

Acknowledgment. This work was financially supported by the Council of Strategic Research (SSF) within the Colloid and Interface Technology (CIT) program. Danisco Cultor is acknowledged for generous support.

References and Notes

(1) Hyde, S. T.; Andersson, S.; Ericsson, B.; Larsson, K. *Z. Kristallogr*. **1984**, *168*, 213.
(2) Engström, S. *Lipid Technol.* **1990**, *2(2)*, 42.
(3) Razumas, V.; Kanapieniene, J.; Nylander, T.; Engström, S.; Larsson, K. *Anal. Chim. Acta* **1994**, *289*, 155.
(4) Landau, E. M.; Rosenbusch, J. P. *Proc. Natl. Acad. Sci. U.S.A.* **1996**, *93*, 14532.
(5) Nollert, P.; Navarro, J.; Landau, E. M. *Acta Crystallogr. D* **2000**, *56*, 781.
(6) Rummel, G.; Hardmeyer, A.; Widmer, C.; Chiu, M. L.; Nollert, P.; Locher, K. P.; Pedruzzi, I.; Landau, E. M.; Rosenbusch, J. P. *J. Struct. Biol.* **1998**, *121*, 82.
(7) Lindell, K.; Engblom, J.; Jonströmer, M.; Carlsson, A.; Engström, S. *Prog. Colloid Polym. Sci.* **1830**, *108*, 111.
(8) Gustafsson, J.; Nylander, T.; Almgren, M.; Ljusberg-Wahren, H. *J. Colloid Interface Sci.* **1999**, *211*, 326.
(9) Landh, T. *J. Phys. Chem.* **1994**, *98*, 8453.
(10) Takahashi, H.; Matsuo, A.; Hatta, I. *Mol. Cryst. Liq. Cryst.* **2000**, *347*, 231.
(11) Engström, S.; Alfons, K.; Rasmusson, M.; Ljusberg-Wahren, H. *Prog. Colloid Polym. Sci.* **1830**, *108*, 93.
(12) Alfons, K.; Engström, S. *J. Pharm. Sci.* **1998**, *87*, 1527.
(13) Ekelund, K.; Engblom, J.; Engström, S. Submitted for publication.
(14) Johansson (now Imberg), A. K.; Linse, P.; Piculell, L.; Engström, S. *J. Phys. Chem. B* **2001**, *105*, 12157.
(15) Assarsson, P.; Eirich, F. R. *Adv. Chem. Ser*. **1968**, 1.
(16) Hong, P. D.; Huang, H. T. *Polymer* **2000**, *41*, 6195.
(17) Stilbs, P. *Prog. NMR Spectrosc.* **1987**, *19*, 1.
(18) Tanner, J. E. *J. Chem. Phys.* **1970**, *52*, 2523.
(19) Stilbs, P.; Paulsen, K.; Griffiths, P. C. *J. Phys. Chem.* **1996**, *100*, 8180.
(20) Evans, D. F.; Wennerström, H. *The Colloidal Domain, where Physics, Chemistry, Biology and Technology meet*, 2nd ed.; Wiley-VCH: New York, 1999.
(21) Evertsson, H.; Stilbs, P.; Lindblom, G.; Engström, S. *Colloids Surf. B* **2002**, *26*, 21.
(22) Luzzati, V.; Tardieu, A.; Gulik-Krzywicki, T.; Rivas, E.; Reiss-Husson, F. *Nature* **1968**, *220*, 485.
(23) Anderson, D.; Wennerström, H.; Olsson, U. *J. Phys. Chem.* **1989**, *93*, 4243.
(24) Balinov, B.; Olsson, U.; Söderman, O. *J. Phys. Chem.* **1991**, *95*, 5931.
(25) Gazeau, D.; Bellocq, A. M.; Roux, D.; Zemb, T. *Europhys. Lett.* **1989**, *9*, 447.
(26) Strey, R.; Jahn, W.; Skouri, M.; Porte, G.; Marignan, J. *Structure and Dynamics of Strongly Interacting Colloids and Supramolecular Aggregates in Solution*; Kluwer Academic Publishers: Dordrecht, The Netherlands, 1992; pp 351−363.
(27) Hyde, S. T. *Langmuir* **1997**, *13*, 842.
(28) Engblom, J. *Chem. Phys. Lipids* **1996**, *84*, 155.
(29) Hyde, S. T.; Andersson, S.; Larsson, K.; Blum, Z.; Landh, T.; Lidin, S.; Ninham, B. W. *The Language of Shape. The Role of Curvature in Condensed Matter*: *Physics, Chemistry and Biology*; Elseiver: Amsterdam, 1997.
(30) Ericsson, B.; Larsson, K.; Fontell, K. *Biochim. Biophys. Acta* **1983**, *729*, 23.
(31) Larsson, K. *Lipids-molecular organization, physical functions and technical applications;* The oily press Ltd.: Dundee, Scotland, 1994.
(32) Borné, J.; Nylander, T.; Khan, A. *Langmuir* **2000**, *16*, 10044.